Theoretical and Applied Mechanics Letters 12 (2022) 100359

Contents lists available at ScienceDirect

Theoretical and Applied Mechanics Letters

journal homepage: www.elsevier.com/locate/taml

Letter

A new dynamic subgrid-scale model using artificial neural network for compressible flow

Han Qi[a,b], Xinliang Li[a,b], Ning Luo[c,*], Changping Yu[a,*]

[a] LHD, Institute of Mechanics, Chinese Academy of Sciences, Beijing 100190, China
[b] School of Engineering Science, University of Chinese Academy of Sciences, Beijing 100049, China
[c] State Key Laboratory for Geomechanics and Deep Underground Engineering,China University of Mining and Technology, Xuzhou 221116, China

ARTICLE INFO

Article history:
Received 20 June 2022
Revised 11 July 2022
Accepted 15 July 2022
Available online 17 July 2022

Keywords:
Subgrid-scale kinetic energy
Eddy-viscosity model
Compressible flow

ABSTRACT

The subgrid-scale (SGS) kinetic energy has been used to predict the SGS stress in compressible flow and it was resolved through the SGS kinetic energy transport equation in past studies. In this paper, a new SGS eddy-viscosity model is proposed using artificial neural network to obtain the SGS kinetic energy precisely, instead of using the SGS kinetic energy equation. Using the infinite series expansion and reserving the first term of the expanded term, we obtain an approximated SGS kinetic energy, which has a high correlation with the real SGS kinetic energy. Then, the coefficient of the modelled SGS kinetic energy is resolved by the artificial neural network and the modelled SGS kinetic energy is more accurate through this method compared to the SGS kinetic energy obtained from the SGS kinetic energy equation. The coefficients of the SGS stress and SGS heat flux terms are determined by the dynamic procedure. The new model is tested in the compressible turbulent channel flow. From the a posterior tests, we know that the new model can precisely predict the mean velocity, the Reynolds stress, the mean temperature and turbulence intensities, etc.

Large-eddy simulation (LES) has been widely used in predicting turbulence and gradually applied to high Reynolds number cases. In LES, the eddy-viscosity model is a very popular model due to its strong stability. The Smagorinsky model (SM) [1] is most popular eddy-viscosity model and is used to many different cases, but the SM shows excessive dissipation and cannot predict the transitional flow. Thus, many different types of eddy-viscosity models are proposed. The wall-adapting local eddy-viscosity model [2] was proposed by Metais, which shows correct behavior in the near-wall region. Vreman obtained a low dissipation model [3] that can predict transitional flow well. Considering the helicity effects, Yu et al. [4,5] supplied a new eddy-viscosity model and it was applied to predict compressible transitional flows Qi et al. proposed an eddy-viscosity model based on the vorticity gradient tensor for rotating turbulent flows [6]. The subgrid-scale (SGS) kinetic energy equation model (k-equation model) is also a type of eddy-viscosity model, which was added the SGS kinetic energy equation to obtain the eddy viscosity. The k-equation model was proposed by Schumann [7] through dimensional analysis and Yoshizawa [8] also obtained the k-equation model by the two-scale direct interaction approximation. Then the k-equation model was applied to compressible flows [9]. Chai et al. [10] supplied a k-equation model where the SGS terms in the equation are modelled independently and the coefficients of the SGS models are determined dynamically . Except for the eddy-viscosity model, the structural model is an important type of SGS models, such as scale-similarity model and gradient model. The scale-similarity model was obtained based on the scale-similarity hypothesis [11]. The gradient model is derived from Taylor expansions for SGS stress [12,13]. The structural model has a high correlation with the real SGS stress but is unstable.

In addition, some LES methods have been introduced to help improving the predicting effects in LES. Using the Germano identity, Germano et al. [14] supplied the dynamic procedure which can dynamically determine the coefficient of the SGS models. Then, Lilly [15], Ghosal et al. [16] and Meneveau et al. [17] obtained a scale-dependent dynamic SGS model and generalized the dynamic procedure to any scalar flux model. Except for the dynamic methods, some other LES methods have been proposed recently. Chen et al. [18] suggested to constrain the SGS stress model by Reynolds stress for LES of incompressible wall-bounded turbulence

* Corresponding authors.
E-mail addresses: nluo@cumt.edu.cn (N. Luo), cpyu@imech.ac.cn (C. Yu).

https://doi.org/10.1016/j.taml.2022.100359

to improve the prediction of the averaged quantities, and then Jiang et al. [19] generalized this method to compressible cases. Domaradzki et al. [20] proposed a new method where the total SGS energy transfer is used to constrain the SGS models and update model constants.

Recently, artificial neural networks (ANNs) have been increasingly applied to develop turbulence models [21]. Ling et al. [22] supplied a new Reynolds stress anisotropic tensor through a new multiplicative-layer neural network with an invariant tensor firstly, which can obtain obvious improvement in simulation result. Using machine learning and through optimal evaluation theory analysis, Vollant et al. [23] obtained a new SGS scalar flux model which can predict results much closer to the DNS results. With the ANN method, Xie et al. [24] supplied the coefficients of the mixed model which combined the Smagorinsky model and the gradient model for compressible isotropic turbulence and the new method have better behaviours than the traditional LES models. Through the relationship between the resolved-scale velocity gradient tensor and the SGS stress tensor, Zhou et al. [25] proposed a new SGS model using the ANN method for isotropic turbulence. Park and Choi [26] obtained an SGS model for LES of turbulent channel flows using a fully connected neural network . The new model can have good performance and is not affected by the grid resolution Yuan et al. [27].

In this paper, a new dynamic eddy-viscosity model (NDKM) is proposed for LES of compressible flow. In this new model, the eddy-viscosity is supplied by the SGS kinetic energy, which is obtained by the infinite series expansion. And the coefficient of the modelled SGS kinetic energy is determined by the artificial neural network.

Filter the Navier-Stokes (N-S) equations and the filtered N-S equations for compressible in LES can be written as

$$\frac{\partial \bar{\rho}}{\partial t}+\frac{\partial \bar{\rho}\tilde{u}_i}{\partial x_j}=0, \tag{1}$$

$$\frac{\partial \bar{\rho}\tilde{u}_i}{\partial t}+\frac{\partial \bar{\rho}\tilde{u}_i\tilde{u}_j}{\partial x_j}=-\frac{\partial \bar{p}}{\partial x_i}+\frac{\partial \tilde{\sigma}_{ij}}{\partial x_j}-\frac{\partial \tau_{ij}}{\partial x_j}, \tag{2}$$

$$\frac{\partial \bar{\rho}\tilde{E}}{\partial t}+\frac{\partial \left(\bar{\rho}\tilde{E}+\bar{p}\right)\tilde{u}_j}{\partial x_j}=-\frac{\partial \tilde{q}_j}{\partial x_j}+\frac{\partial \tilde{\sigma}_{ij}\tilde{u}_i}{\partial x_j}-\frac{\partial C_pQ_j}{\partial x_j}-\frac{\partial J_j}{\partial x_j}, \tag{3}$$

where

$$\tau_{ij}=\overline{\rho}\left(\widetilde{u_iu_j}-\tilde{u}_i\tilde{u}_j\right), \tag{4}$$

$$Q_j=\overline{\rho}\left(\widetilde{u_jT}-\tilde{u}_j\tilde{T}\right), \tag{5}$$

$$\tilde{q}_j=\frac{C_p\mu\left(\tilde{T}\right)}{Pr}\frac{\partial \tilde{T}}{\partial x_j}, \tag{6}$$

$$J_j=\frac{1}{2}\overline{\rho}\left(\widetilde{u_iu_iu_j}-\widetilde{u_iu_i}\tilde{u}_j\right), \tag{7}$$

$$\overline{\rho}\tilde{E}=\overline{\rho}C_v\tilde{T}+\frac{1}{2}\overline{\rho}\tilde{u}_i\tilde{u}_i+\overline{\rho}k_{sgs}, \tag{8}$$

$$\overline{\rho}k_{sgs}=\frac{1}{2}\overline{\rho}(\widetilde{u_iu_i}-\tilde{u}_i\tilde{u}_i), \tag{9}$$

$$\tilde{\sigma}_{ij}=2\mu\left(\tilde{T}\right)\left(\tilde{S}_{ij}-\frac{1}{3}\delta_{ij}\tilde{S}_{kk}\right), \tag{10}$$

$$\tilde{S}_{ij}=\frac{1}{2}\left(\frac{\partial \tilde{u}_i}{\partial x_j}+\frac{\partial \tilde{u}_j}{\partial x_i}\right). \tag{11}$$

And $\bar{(\cdot)}$represents spatial filtering with a low-pass filter at scale Δ and $\tilde{(\cdot)}$ represents density-weighted (Favre) filtering ($\tilde{\phi}=\frac{\overline{\rho\phi}}{\bar{\rho}}$). In the filtered N-S equations, $\bar{\rho}$, $\tilde{u}_i$, $\tilde{T}$, $\bar{p}$ and $\tilde{E}$ are the filtered density, velocity, pressure and total energy, respectively. The filtered pressure is determined by $\bar{p}=\bar{\rho}R\tilde{T}$, where R is the specific gas constant. In the equations, Pr is the molecular Prandtl number and the molecular viscosity μ takes the form $\mu=\frac{1}{Re}\left(\frac{\tilde{T}}{\tilde{T}_\infty}\right)^{3/2}\frac{\tilde{T}_\infty+\tilde{T}_s}{\tilde{T}+\tilde{T}_s}$ according to Sutherland's law, in which T_s is 110.3 K, the Reynolds number Re takes the form $Re=\rho_\infty U_\infty L/\mu_\infty$.

Based on Boussinesq type hypothesis, the eddy-viscosity model can be written as

$$\tau_{ij}^{\mathrm{mod}}-\frac{1}{3}\delta_{ij}\tau_{kk}^{\mathrm{mod}}=-2\mu_{sgs}\left(\tilde{S}_{ij}-\frac{1}{3}\delta_{ij}\tilde{S}_{kk}\right), \tag{12}$$

where τ_{kk}^{mod} is the isotropic part of the SGS stress model and μ_{sgs} is the SGS eddy viscosity. And it can be known $\tau_{kk}=2\bar{\rho}k_{sgs}$.

For the SGS heat flux model, the commonly used SGS diffusion model is as

$$Q_j^{\mathrm{mod}}=-\frac{\mu_{sgs}}{\mathrm{Pr}_{sgs}}\frac{\partial \tilde{T}}{\partial x_j}, \tag{13}$$

and Pr_{sgs} is the SGS Prandtl number.

In the compressible dk-equation model, the modelled SGS stress and SGS heat flux can be written as

$$\tau_{ij}-\frac{2}{3}\overline{\rho}k_{sgs}\delta_{ij}=-2C_s\Delta\overline{\rho}\sqrt{k_{sgs}}\left(\tilde{S}_{ij}-\frac{1}{3}\delta_{ij}\tilde{S}_{kk}\right), \tag{14}$$

$$Q_j=-\frac{C_s\Delta\overline{\rho}\sqrt{k_{sgs}}}{Pr_{sgs}}\frac{\partial \tilde{T}}{\partial x_j}. \tag{15}$$

In compressible dk-equation model, k_{sgs} is solved by the SGS kinetic energy equation. In the following, we will introduce another method to obtain k_{sgs}.

First, we introduce the infinite series expansion [28] as

$$\begin{aligned}\overline{fg}-\bar{f}\bar{g}=&\alpha\frac{\partial \bar{f}}{\partial x_k}\frac{\partial \bar{g}}{\partial x_k}+\frac{1}{2!}(\alpha)^2\frac{\partial^2 \bar{f}}{\partial x_k\partial x_l}\frac{\partial^2 \bar{g}}{\partial x_k\partial x_l}\\&+\frac{1}{3!}(\alpha)^3\frac{\partial^3 \bar{f}}{\partial x_k\partial x_l\partial x_m}\frac{\partial^3 \bar{g}}{\partial x_k\partial x_l\partial x_m}+\dots,\end{aligned} \tag{16}$$

where

$$\alpha(y)=\int_{-\infty}^{\infty}2x^2G(x,y)\mathrm{d}x. \tag{17}$$

In Eq. (17), $G(x,y)$ is the kernel of the filter and designated as the box filter in *a priori* and the grid filter in *a posterior*.

When applying the infinite series expansion to SGS kinetic energy, one can obtain

$$\begin{aligned}\overline{\rho}k_{sgs}=&\frac{1}{2}\overline{\rho}(\widetilde{u_iu_i}-\tilde{u}_i\tilde{u}_i)=C_k\Delta_k^2\overline{\rho}\frac{\partial \tilde{u}_i}{\partial x_k}\frac{\partial \tilde{u}_i}{\partial x_k}\\&+\frac{1}{2!}\left(C_k^2\Delta_k^2\Delta_l^2\right)\overline{\rho}\frac{\partial^2 \tilde{u}_i^2}{\partial x_k\partial x_l}\frac{\partial^2 \tilde{u}_i^2}{\partial x_k\partial x_l}+\cdots,\end{aligned} \tag{18}$$

where $\mathrm{C_k}$ is the coefficient and Δ_k is the grid width in the x_k direction.

For avoiding the complexity of additional boundary conditions and due to the other higher-order terms are small enough compared to the first term, we only reserve the first term and it can be expressed as

$$\overline{\rho}k_{sgs}\approx C_k\Delta_k^2\overline{\rho}\frac{\partial \tilde{u}_i}{\partial x_k}\frac{\partial \tilde{u}_i}{\partial x_k}, \tag{19}$$

For obtaining the coefficient C_k, we will use artificial neural network in the next part.

The coefficient C_s and Pr_{sgs} are determined dynamically by the Germano identity. For any term $a=\overline{\alpha\beta}-\overline{\alpha}\overline{\beta}$, we assume that $A=$

$\widehat{\overline{\alpha}\overline{\beta}} - \widehat{\overline{\alpha}}\widehat{\overline{\beta}}$ holds on the test filter level, where $\hat{}$ denotes test filtering. The Germano identity is then defined by $L = A - \hat{a} = \widehat{\overline{\alpha}\overline{\beta}} - \widehat{\overline{\alpha}}\widehat{\overline{\beta}}$. Assume that the model for a is $a = Cm$, where m is a function of the resolved (grid filter level) quantities; then at the test filter level, $A = CM$, where M takes similar form to m but is a function of the test-filtered quantities. Substituting the models for A and a, the Germano identity becomes

$$L = \widehat{\overline{\alpha}\overline{\beta}} - \widehat{\overline{\alpha}}\widehat{\overline{\beta}} = C\left(M - \hat{m}\right). \tag{20}$$

The model coefficient C can be solved dynamically as

$$C = \frac{\widehat{\overline{\alpha}\overline{\beta}} - \widehat{\overline{\alpha}}\widehat{\overline{\beta}}}{M - \hat{m}}. \tag{21}$$

The coefficient C varies with time and space. To avoid computational instability, C is regularized using a combination of least-square method and volume averaging. For the coefficient of SGS stress C_s is

$$C_s\Delta^2 = \frac{1}{2}\frac{\langle L_{ij}^* M_{ij}^* \rangle}{\langle M_{ij}^* M_{ij}^* \rangle}, \tag{22}$$

where

$$L_{ij} = \left(\frac{\widehat{\overline{\rho}\overline{u}_i\overline{\rho}\overline{u}_j}}{\overline{\rho}}\right) - \frac{\widehat{\overline{\rho}\overline{u}_i}\widehat{\overline{\rho}\overline{u}_j}}{\widehat{\overline{\rho}}}, \tag{23}$$

$$L_{ij}^* = L_{ij} - \frac{1}{3}\delta_{ij}L_{kk}, \tag{24}$$

$$M_{ij}^* = \bar{\rho}K\left(\tilde{S} - \frac{1}{3}\delta_{ij}\tilde{S}_{kk}\right) - \hat{\bar{\rho}}\left(\frac{\hat{\Delta}}{\Delta}\right)k_{sgs}\left(\tilde{S}_{ij} - \frac{1}{3}\delta_{ij}\tilde{S}_{kk}\right) \tag{25}$$

$$K = \widehat{k_{sgs}} + \frac{1}{2}\left(\widehat{\tilde{u}_i\tilde{u}_i} - \hat{\tilde{u}}_i\hat{\tilde{u}}_i\right). \tag{26}$$

For the coefficient of SGS heat flux model, it can be determined dynamically as

$$Pr_{sgs} = \frac{\langle M_j^\theta M_j^\theta \rangle}{\langle L_j^\theta M_j^\theta \rangle}, \tag{27}$$

where

$$L_j^\theta = \bar{\rho}\widehat{\tilde{u}_j\tilde{T}} - \frac{1}{\hat{\bar{\rho}}}\hat{\bar{\rho}}\hat{\tilde{u}}_j\hat{\bar{\rho}}\hat{\tilde{T}}, \tag{28}$$

$$M_j^\theta = \bar{\rho}\nu_{sgs}\widehat{\frac{\partial\tilde{T}}{\partial x_j}} - \hat{\bar{\rho}}\hat{\nu}_{sgs}\frac{\partial\hat{\tilde{T}}}{\partial x_j}. \tag{29}$$

In our study, we use an ANN to construct the coefficient C_k in compressible turbulent channel flow. The data selected for training and testing in this study are obtained from the direct numerical simulation (DNS) data of a temporally compressible isothermal-wall turbulent channel flow [29]. In this case, the Mach number $Ma = 1.5$, the Reynolds number $Re = 3000$, and the friction Reynolds number $Re_\tau = u_\tau\delta/\nu = 220$ (u_τ and δ are the friction velocity and the half width of the channel). The computation domain for the DNS of channel flow is a box with a size of $4\pi \times 2 \times 4/3\pi$, and the grids for DNS are $900 \times 201 \times 300$ and $\Delta x^+ \times \Delta y^+_{wall} \times \Delta z^+ = 3 \times 0.32 \times 3$, where Δx^+, Δy^+_{wall}, and Δz^+ ($\Delta x_i^+ = \Delta x_i u_\tau/\nu$) are the mesh spacings of wall units in streamwise, wall-normal, and spanwise directions. During the course of training and testing, the DNS data are filtered in streamwise and spanwise directions with a box filter. The input features of the ANN are critical to the performance of predicting the coefficient C_k. A set of input variables are dimensionless quantities, where several variables may be selected in compressible wall-bounded turbulence, such as

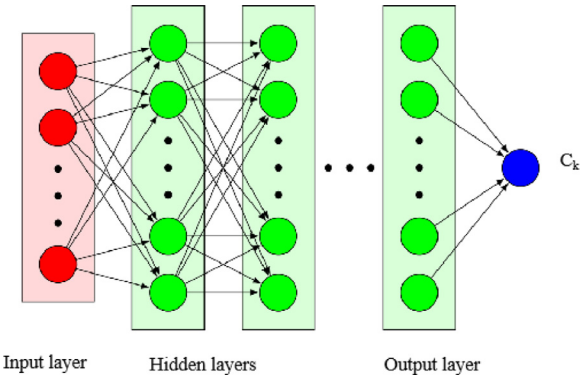

Fig. 1. Schematic diagram of the artificial neural network for predicting the model coefficient C_k.

Table 1
A set of inputs and outputs for different ANN models.

Model	ANN1	ANN2	ANN3
Inputs	Δ^+, y^+	Δ_l^+, y^+	Re_Δ, y^+
Outputs	C_k	C_k	C_k

Δ^+, y^+, Re_Δ, and Δ_l^+. In this paper, $\Delta^+ = \bar{\rho}_w\tilde{u}_\tau\Delta/\mu_w$ is the normalized filter width, $y^+ = \bar{\rho}_w\tilde{u}_\tau y/\mu_w$ is the dimensionless normal distance, $Re_\Delta = \rho_w|\tilde{S}|\Delta^2/\mu_w$ is the mesh Reynolds number, and $\Delta_l^+ = \Delta/l$, $l = [\mu_w^2/(2\bar{\rho}_w^2\langle\tilde{S}_{ij}\tilde{S}_{ij}\rangle)]^{1/4}$. The filtered wall friction velocity is $\tilde{u}_\tau = \sqrt{\tau_w/\bar{\rho}_w}$, where $\tau_w = \mu_w\frac{\partial\tilde{u}}{\partial y}$ is the wall shear stress and $\langle\cdot\rangle$ is denoted as the spatial average along the homogeneous directions. Figure 1 shows schematic diagram of the artificial neural network for predicting the model coefficients C_k. Table 1 shows a set of inputs and outputs for different ANN models. In this paper, a total of four layers (an input layer, two hidden layers and an output layer) with neurons in the ratio M: 100: 100: 1 and M is the number of input variables listed in Table 1. The activation functions of the hidden layers and output layer are the hyperbolic tangent function ($\sigma_h(x) = (e^x - e^{-x})/(e^x + e^{-x})$) and linear function ($\sigma_o(x) = x$). The mean-squared error (MSE) function is chosen as the loss function of the ANN ($L = \langle(C_k^{true} - C_k^{pred})^2\rangle$, where C_k^{true} and C_k^{pred} denote the true and predicted values of the ANN.)

In this study, we select 2×10^4 samples from 20 snapshots of the filtered DNS data with a ratio of the filter width $\Delta/\Delta_{\mathrm{DNS}}$ ranging from 2 to 20 ($\Delta/\Delta_{\mathrm{DNS}} \in \{2, 4, \ldots, 20\}$). The cross-validation strategy is used and the dataset is divided into a training set and testing set to suppress parameter overfitting of the ANN. We randomly extract seventy percent of the samples from the total dataset and are used as the training set, while the others are used for testing. The weights of the ANN are initialized by the Glorot-uniform algorithm and optimized by the Adam algorithm [30] for 1×10^4 iterations, with a batch size and learning rate of 1000 and 0.01, respectively. To determine the optimal hyperparameters, such as the numbers of layers and neurons and the types of activation functions, we choose the grid search method as the hyperparameter pruning method of the ANN.

For seeing the rationality of the selected hyperparameters, in Table 2, we supply the correlation coefficient $C(C_k)$, the relative error $E_r(C_k)$, and the ratio of the root-mean-square value $R(C_k)$, which are defined, respectively, as

$$C(C_k) = \frac{\left\langle\left(C_k^{real} - \left\langle C_k^{real}\right\rangle\right)\left(C_k^{\mathrm{mod}\,el} - \left\langle C_k^{\mathrm{mod}\,el}\right\rangle\right)\right\rangle}{\left\langle\left(C_k^{real} - \left\langle C_k^{real}\right\rangle\right)^2\right\rangle^{1/2}\left\langle\left(C_k^{\mathrm{mod}\,el} - \left\langle C_k^{\mathrm{mod}\,el}\right\rangle\right)^2\right\rangle^{1/2}}, \tag{30}$$

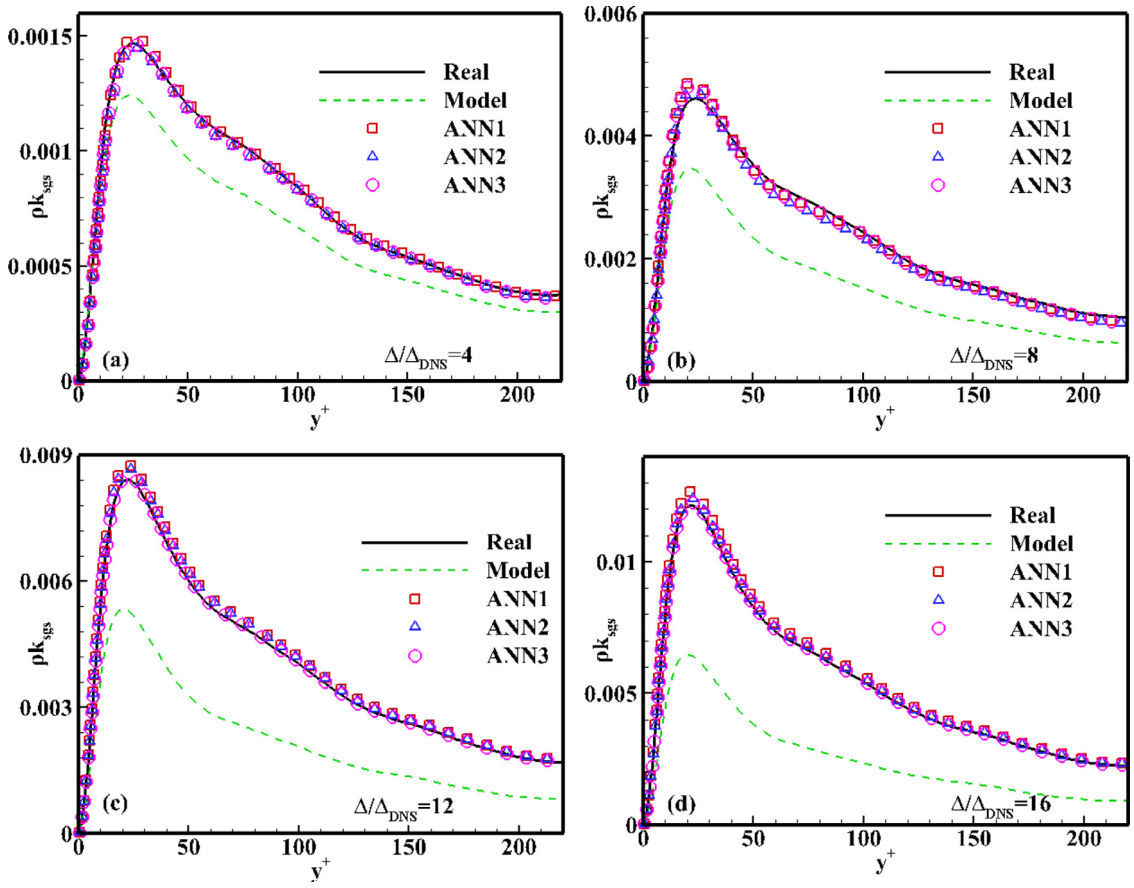

Fig. 2. Comparisons of the coefficient C_k reconstructed by different ANN models along the normal direction with different filter widths: (**a**) $\Delta/\Delta_{DNS}=4$; (**b**) $\Delta/\Delta_{DNS}=8$; (**c**) $\Delta/\Delta_{DNS}=12$; (**d**) $\Delta/\Delta_{DNS}=16$ (the Model in the pictures means that C_k is 1/12 and $\bar{\rho}k_{sgs}\approx\frac{1}{24}\Delta_k^2\bar{\rho}(\partial\tilde{u}_i/\partial x_k)^2$).

Table 2
Correlation coefficient(C), relative error(Er), and ratio of root-mean-square value

Dataset\$C(C_k)$	ANN1	ANN2	ANN3
Training	0.922	0.932	0.933
Testing	0.911	0.913	0.919
Dataset\$E_r(C_k)$	ANN1	ANN2	ANN3
Training	0.112	0.109	0.105
Testing	0.123	0.122	0.118
Dataset\$R(C_k)$	ANN1	ANN2	ANN3
Training	0.921	0.931	0.932
Testing	0.901	0.903	0.909

$$E_r(C_k)=\frac{\left\langle\left(C_k^{real}-C_k^{\mathrm{mod}\,el}\right)^2\right\rangle^{1/2}}{\left\langle\left(C_k^{real}\right)^2\right\rangle^{1/2}}, \tag{31}$$

$$R(C_k)=\frac{\left\langle\left(C_k^{\mathrm{mod}\,el}-\left\langle C_k^{\mathrm{mod}\,el}\right\rangle\right)^2\right\rangle^{1/2}}{\left\langle\left(C_k^{real}-\left\langle C_k^{real}\right\rangle\right)^2\right\rangle^{1/2}}. \tag{32}$$

From the results in Table 2, we know that the selected hyper-parameters are reasonable and the ANN models are well trained.

(R) of the coefficient C_k in different datasets for different ANN models.

Figure 2 shows comparisons of the coefficient C_k reconstructed by different ANN models along the normal direction with different filter widths. From the figures, we know that the modelled SGS kinetic energy modified by the ANNs models can have similar results and have good agreement with the DNS results. We choose the ANN3 model in the following testing because the ANN3 model has the best behaviours in the three ANN models.

In this section, the new model is tested in compressible turbulent channel flow. The case setting of the LES in this part is same as that of the DNS in previous part. The governing equations are solved by a high-precision non-dimensional finite difference solver in Cartesian coordinates: the third-order R- scheme is chosen as the time integrating method, and a sixth-order central difference scheme is used for the discretization of both the convective and viscous terms. The grid filter width is $\Delta=(\Delta_x\Delta_y\Delta_z)^{1/3}$ with Δ_x, Δ_y and Δ_z representing the local grid width, and the test-filter width is set as 2Δ. Table 3 shows the grid setting and the main parameters for the simulations in the compressible turbulent channel flow.

Figure 3 shows the profiles of Van Driest transformed mean velocity ($U_{vd}=\int_0^U\sqrt{\langle\rho\rangle/\rho_w}d\langle U\rangle$) and the mean temperature $T_{av}^+=(T_w-\langle T\rangle)/T_\tau$ obtained from DNS, the NDKM and the dk-equation model. $T_\tau=B_qT_w$ is the friction temperature, $B_q=q_w/(\rho_wc_pu_\tau T_w)$ is the nondimensional heat flux, and q_w is the wall-normal heat flux. From the figures, we know that the NDKM can have perfect agreement with the DNS results, but the dk-equation model shows deviations at $y^+>30$.

The profiles of the total Reynolds stress and the total turbulent heat flux from DNS and different SGS models are shown in Fig. 4. In Fig. 4a, the NDKM can have perfect behavior at almost regions but the dk-equation model shows worse results. In Fig. 4b, the NDKM has good performance but the results from the NDKM are a little higher than results from DNS at $15<y^+<30$. The dk-equation model still shows deviation with DNS.

Table 3
The grid setting and the main parameters for the simulations in the compressible turbulent channel flow ($Ma = 1.5$ and $Re = 3000$).

	Grids	Δx^+	Δy_w^+	Δz^+	Re_τ	Ma_τ	$-B_q$
DNS	900×201×300	2.99	0.32	2.99	220	0.0815	0.0445
dk-equation model	48×65×48	57.6	1.07	18.2	210	0.0805	0.0431
NDKM	48×65×48	57.5	1.07	18.1	216	0.0813	0.0442

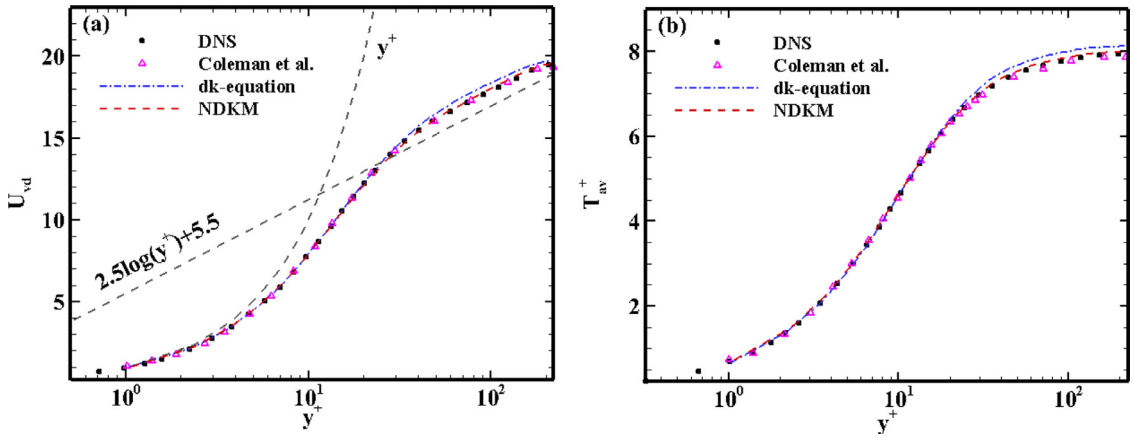

Fig. 3. The profiles of Van Driest transformed mean velocity and the mean temperature from different SGS models and results from DNS is as comparison ('Coleman et al.' is data from Coleman et al. [29]).

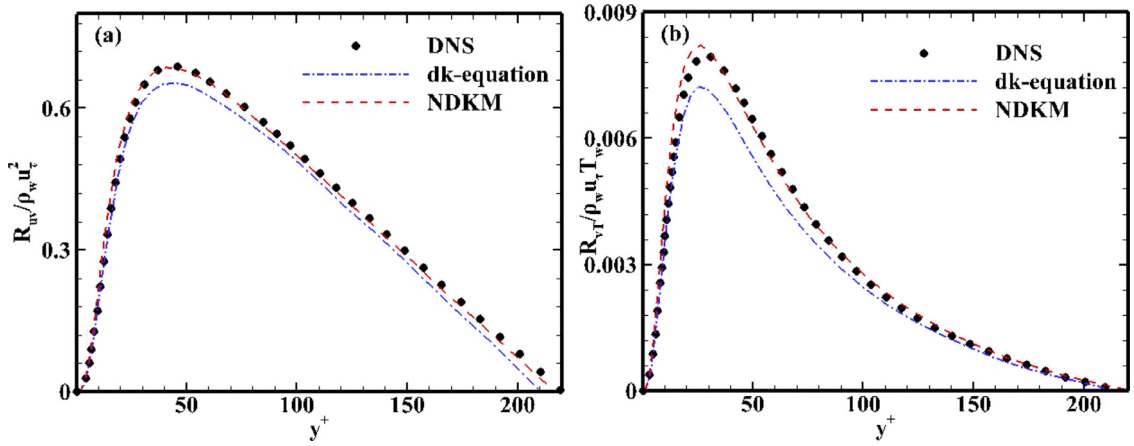

Fig. 4. The profiles of the total Reynolds stress normalized by ρ_w and u_τ, and the total turbulent heat flux normalized by ρ_w, u_τ and T_w from DNS and different SGS models.

The profiles of the resolved turbulence intensities from DNS, the NDKM and dk-equation model are shown in Fig. 5a, 5b and 5c. From the figures, we know that the NDKM shows better predictions than the dk-equation at almost regions. Figure 5d shows the turbulent kinetic energy from DNS and different SGS models. In the figure, we know that the NDKM can well predict the total turbulent kinetic energy and the SGS part. We also can infer that the NDKM can obtain better SGS kinetic energy than the dk-equation model.

Figure 6 shows that the profiles of the resolved RMS density fluctuations and the resolved RMS temperature fluctuations from DNS and different SGS models. From the figures, we know that the NDKM can well predict the resolved RMS density fluctuations and the resolved RMS temperature fluctuations. The dk-equation model can also show good behaviours but still behaves a little worse than the NDKM.

Next, we will test the new model in the case of $Ma = 3.0$ and $Re = 4880$. The size of the computational domain, the Prandtl number Pr, the boundary conditions, the ratio of specifific heats and the setting of LES solver are the same with the case of $Ma = 1.5$ and $Re = 3000$. The grid setting and the main parameters for this case are shown in Table 4.

Figure 7 shows the profiles of the Van Driest transformed mean velocity U_{vd} and mean temperature T^+_{av} obtained from different SGS models and DNS. Figure 8 shows the profiles of the total Reynolds stress and the turbulent heat flux from different SGS models and DNS. From the figures, we can see that the NDKM can also obtain better results than dk-equation model in the case of higher Mach number.

In this paper, we propose a new eddy-viscosity model for large-eddy simulation of compressible flow. In this new model, the eddy viscosity is obtained by the subgrid-scale kinetic energy. The SGS kinetic energy is an unclosed term and for resolving this quantity, we apply the infinity series expansion to it. Since the other higher-order terms are small enough compared to the first term, and for avoiding the complexity of additional boundary conditions, the first term of the expanded quantity is reserved as the modelled SGS kinetic energy. And the coefficient of the modelled SGS kinetic energy is determined by the artificial neural network. The coefficients of the eddy-viscosity model are determined dynamically

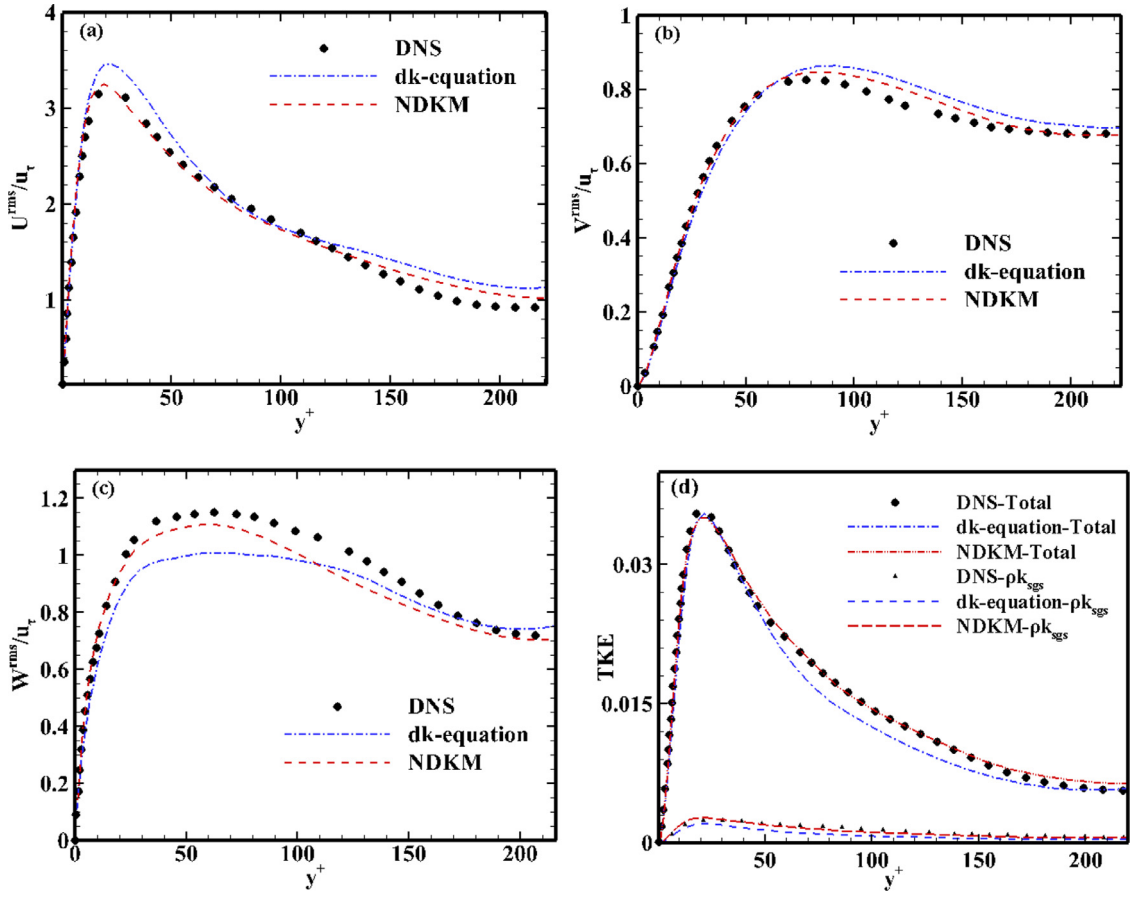

Fig. 5. The profiles of the resolved turbulence intensities normalized by the friction velocity u_τ and the turbulent kinetic energy from DNS and different SGS models: (**a**) Streamwise turbulence intensity; (**b**) Wall-normal turbulence intensity; (**c**) Spanwise turbulence intensity; (**d**) The turbulent kinetic energy.

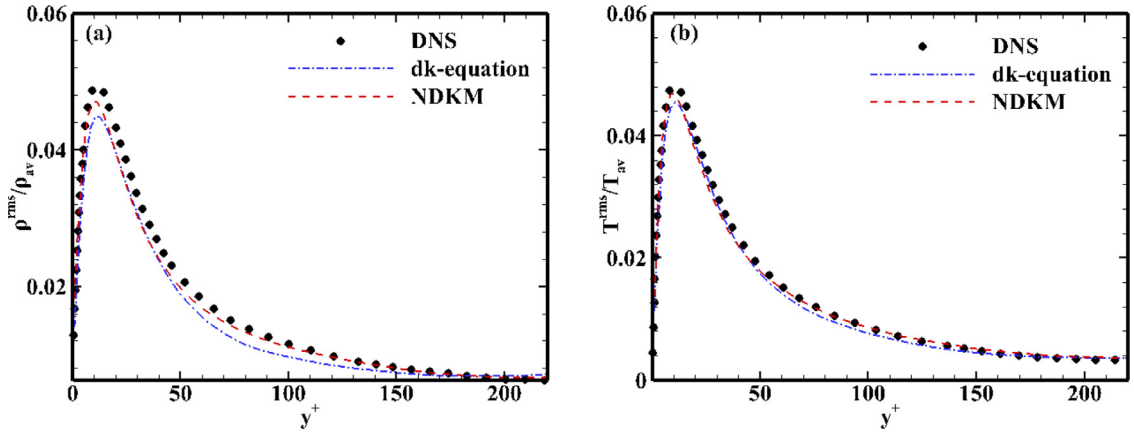

Fig. 6. The profiles of the resolved RMS density fluctuations normalized by averaged density ρ_{av}, and the resolved RMS temperature fluctuations normalized by averaged temperature T_{av} from DNS and different SGS models: (**a**) density fluctuations; (**b**) temperature fluctuations.

Table 4
The grid setting and the main parameters for the simulations in the compressible turbulent channel flow ($Ma = 3.0$ and $Re = 4880$).

	Grids	Δx^+	Δy_w^+	Δz^+	Re_τ	Ma_τ	$-B_q$
d*k*-equation model	86×97×86	66.5	1.44	19.5	448	0.108	0.129
NDKM	86×97×86	66.4	1.44	19.4	450	0.110	0.131

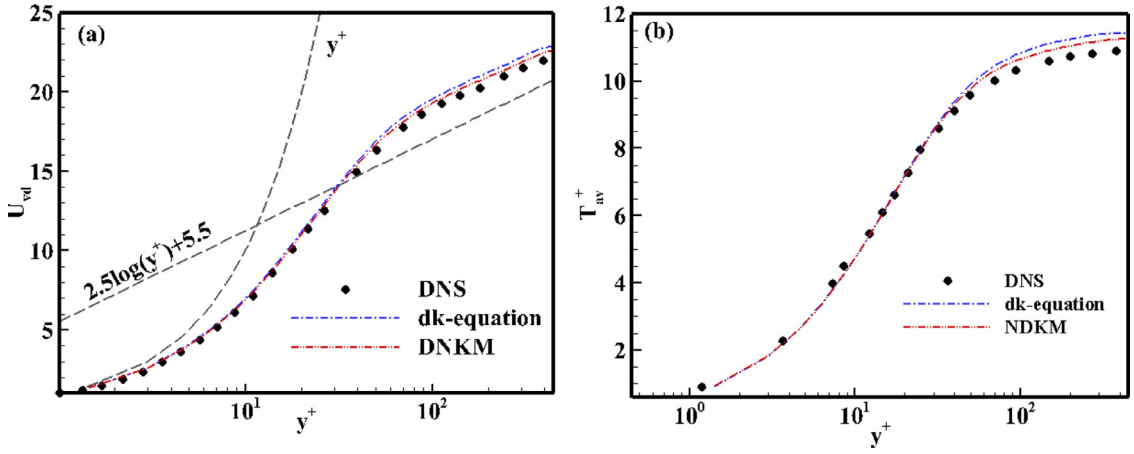

Fig. 7. The profiles of the van Driest transformed mean velocity U_{vd} and mean temperature T^{+}_{av} obtained from different SGS models and DNS. The DNS results are from Coleman et al. [29].

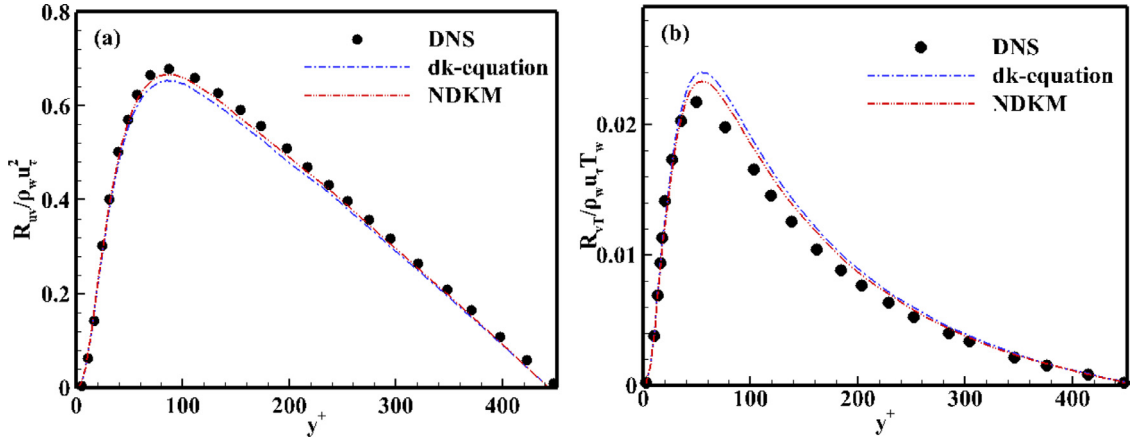

Fig. 8. The profiles of the total Reynolds stress and the turbulent heat flux normalized by ρ_w, u_τ and T_w from different SGS models and DNS. The DNS results are from Coleman et al. [29].

by the Germano identity. The new model is tested in compressible turbulent channel flow and it shows that the new model can show better behavior than the dynamic SGS kinetic energy equation model, including the mean velocity profile, the mean temperature profile, the RMS quantities, the total Reynolds stress and the turbulent heat flux, etc. Compared to the SGS kinetic energy equation model, the NDKM can obtain precise SGS kinetic energy and has higher computational efficiency.

In summary, a new SGS eddy-viscosity model is proposed using the artificial neural network to predict the SGS kinetic energy for LES of compressible flow, and it can present good results. In future researches, the new model will be applied to high Mach number flows in complex geometries.

Declaration of Competing Interest

The authors declare that they have no competing interests and all author(s) read and approved the final manuscript.

Acknowledgements

This work was supported by the National Key Research and Development Program of China (Grant Nos. 2020YFA0711800, 2019YFA0405302) and NSFC Projects (Grant Nos. 12072349, 91852203), National Numerical Windtunnel Project, Science Challenge Project (Grant No. TZ2016001), and Strategic Priority Research Program of Chinese Academy of Sciences (Grant No. XDC01000000). The authors thank the National Supercomputer Center in Tianjin (NSCC-TJ) and the National Supercomputer Center in GuangZhou (NSCC-GZ) for providing computer time .

References

[1] J. Smagorinsky, General circulation experiments with the primitive equations: I. the basic experiment, Mon. Weather Rev 91 (1963) 99–164.
[2] A.W. Vreman, An eddy-viscosity subgrid-scale model for turbulent shear flow: algebraic theory and applications, Phys. Fluids. 16 (2004) 3670–3681.
[3] F. Nicoud, F. Ducros, Subgrid-scale stress modelling based on the square of the velocity gradient tensor, Flow, Turbulence Combust 63 (1999) 183–200.
[4] C. Yu, R. Hong, Z. Xiao, et al., Subgrid-scale eddy viscosity model for helical turbulence, Phys. Fluids. 25 (2013) 095101.
[5] H. Zhou, X. Li, H. Qi, et al., Subgrid-scale model for large-eddy simulation of transition and turbulence in compressible flows, Phys. Fluids 31 (2019) 125118.
[6] H. Qi, X.L. Li, Yu, Subgrid-scale model based on the vorticity gradient tensor for rotating turbulent flows, Acta Mech. Sin. 36 (2020) 692–700.
[7] U. Schumann, Subgrid scale model for finite difference simulations of turbulent flows in plane channels and annuli, J. Comput. Phys. 18 (1975) 376–404.
[8] H.K. Yoshizawa, A statistically-derived subgrid-scale kinetic energy model for the large-eddy simulation of turbulent flows, J. Phys. Soc. Jpn. 54 (1985) 2834–2839.
[9] Franklin Genin, Suresh Menon, Dynamics of sonic jet injection into supersonic crossflow, J. Turbulence 11 (2010) 30.
[10] X. Chai, K Mahesh, Dynamic *k*-equation model for large-eddy simulation of-compressible flows, J. Fluid Mech. 699 (2012) 385–413.
[11] J. Bardina, J. Ferziger, W Reynolds, in: Improved Subgrid-Scale Models for Large-Eddy Simulation, AIAA Paper, 1980, pp. 80–1357.
[12] R.A. Clark, J.H. Ferziger, W.C Reynolds, Evaluation of subgrid-scale models using an accurately simulated turbulent flow, J. Fluid Mech. 91 (1979) 1–16.
[13] B. Vreman, B. Geurts, H Kuerten, Large-eddy simulation of the temporal mixing layer using the clark model, Theor. Comput. Fluid Dyn. 8 (1996) 309–324.

[14] M. Germano, U. Piomelli, P. Moin, et al., A dynamic subgrid-scale eddy viscosity model, Phys. Fluids A. 3 (1991) 1760–1765.
[15] D.K. Lilly, A proposed modification of the germano subgrid-scale closure method, Phys. Fluids A. 238 (1992) 633–635.
[16] S. Ghosal, T.S. Lund, P. Moin, et al., A dynamic localization model for large-eddy simulation of turbulent flows, J. Fluid Mech. 286 (1995) 229–255.
[17] C. Meneveau, T.S. Lund, W.H Cabot, A lagrangian dynamic subgrid-scale model of turbulence, J. Fluid Mech. 319 (1996) 353–385.
[18] S. Chen, Z. Xia, S. Pei, et al., Reynolds-stressconstrained large-eddy simulation of wall-bounded turbulent flows, J. Fluid Mech. 703 (2012) 1–28.
[19] Z. Jiang, Z. Xiao, Y. Shi, Constrained large-eddy simulation of wall-bounded compressible turbulent flows, Phys. Fluids 25 (2013) 106102.
[20] J.Andrzej Domaradzki, Large eddy simulations of high Reynolds number turbulence based on interscale energy transfer among resolved scales, Phys. Rev. Fluids. 6 (2021) 044609.
[21] X.W Guo, Z.H. Xia, S.Y Chen, Practical framework for data-driven RANS modeling with data augmentation, Acta Mech. Sin. 37 (2021) 1748–1756.
[22] J. Ling, A. Kurzawski, J.P Templeton, Reynolds averaged turbulence modelling using deep neural networks with embedded invariance, J. Fluid Mech. 807 (2016) 155–166.
[23] V. Vollant, G. Balarac, C Corre, Subgrid-scale scalar flux modelling based on optimal estimation theory and machine-learning procedures, J. Turbulence. 18 (2017) 854–878.
[24] C. Xie, J. Wang, H. Li, et al., Artificial neural network mixed model for large eddy simulation of compressible isotropic turbulence, Phys. Fluids. 31 (2019) 085112.
[25] Z. Zhou, G. He, S. Wang, et al., Subgrid-scale model for large-eddy simulation of isotropic turbulent flows using an artificial neural network, Comput. Fluids. 195 (2019) 104319.
[26] J. Park, H. Choi, Toward neural-network-based large eddy simulation: application to turbulent channel flow, J. Fluid Mech. 914 (2021) A16.
[27] Z.L. Yuan, Y.P. Wang, C.Y. Xie, et al., Deconvolutional artificial-neural-network framework for subfilter-scale models of compressible turbulence, Acta Mech. Sin. 37 (2021) 1773–1785.
[28] K. Bedford, W. Yeo, Conjuctive filtering procedures in surface water flow and transport, in: Large Eddy Simulation of Complex Engineering and Geophysical Flows, Cambridge University Press, 1993, pp. 513–539.
[29] G.N. Coleman, J. Kim, R.D. Moser, A numerical study of turbulent supersonic isothermal-wall channel flow, J. Fluid Mech. 305 (1995) 159–183.
[30] D.P. Kingerma, J. Ba, A method for stochastic optimization, (2019) arXiv:1412.6980.